Thermal Emission from Cosmic Ray Modified Shocks

Dan Patnaude
SAO

Don Ellison (NCSU)
Pat Slane (SAO)

DSA: A BRIEF OVERVIEW

- Efficient diffusive shock acceleration lowers the shock temperature and raises the postshock density (Jones & Ellison, 1991; Berezhko & Ellison, 1999)

- The nonequilibrium ionization is dependent upon both the shock temperature and the shock density through their relation to the electron temperature, T_e, and electron density, n_e

- A number of Galactic SNRs show both thermal and nonthermal emission behind the forward shock, including SN1006 (Vink et al. 2003; Bamba et al. 2008) and Tycho (Hwang et al. 2002; Cassam-Chenaï et al. 2007)

- In SNR RX J 1713.7-3946, the lack of thermal X-ray emission is an important constraint on the ambient density and significantly impacts models for TeV emission (Slane et al. 1999; Ellison et al. 2001, Aharonian et al. 2007; Katz & Waxman 2008)

Evidence for Efficient DSA in SNRs

- Morphological evidence:

  Efficient shock acceleration softens the equation of state in the shocked gas

  In Tycho, the location of the contact discontinuity in relation to the blastwave suggests that the blastwave has lost energy to cosmic rays

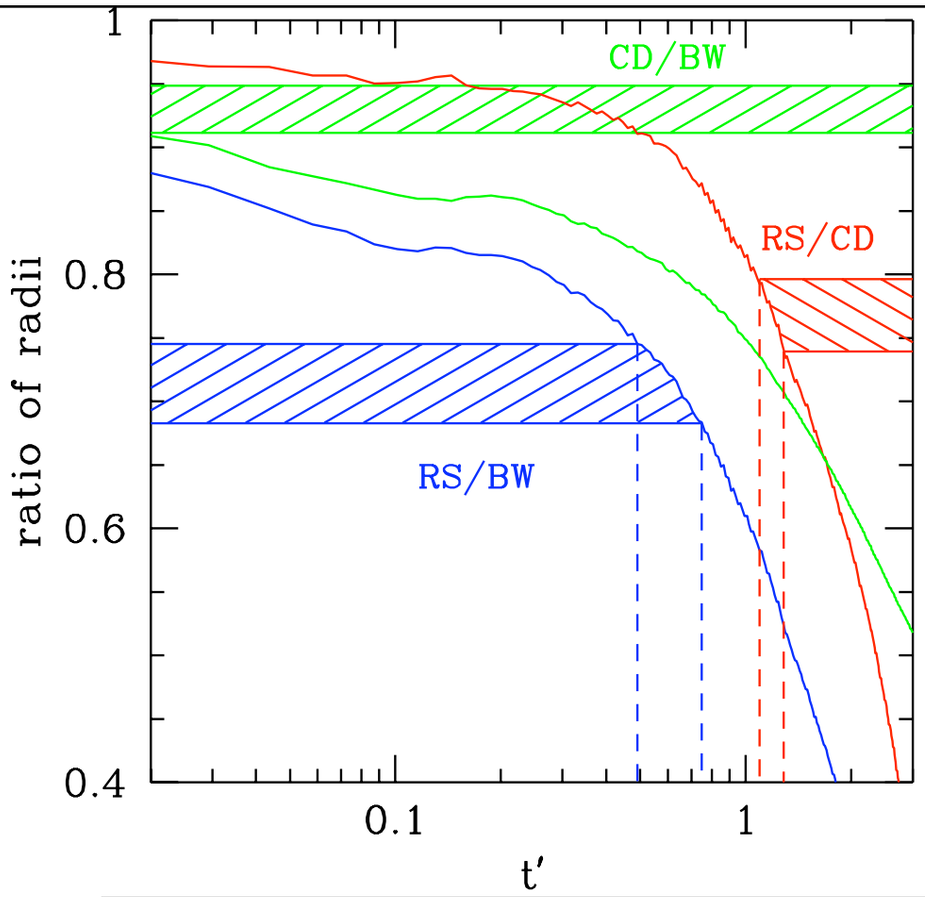

Time evolution for the of Tycho (Warren et al. 2005).

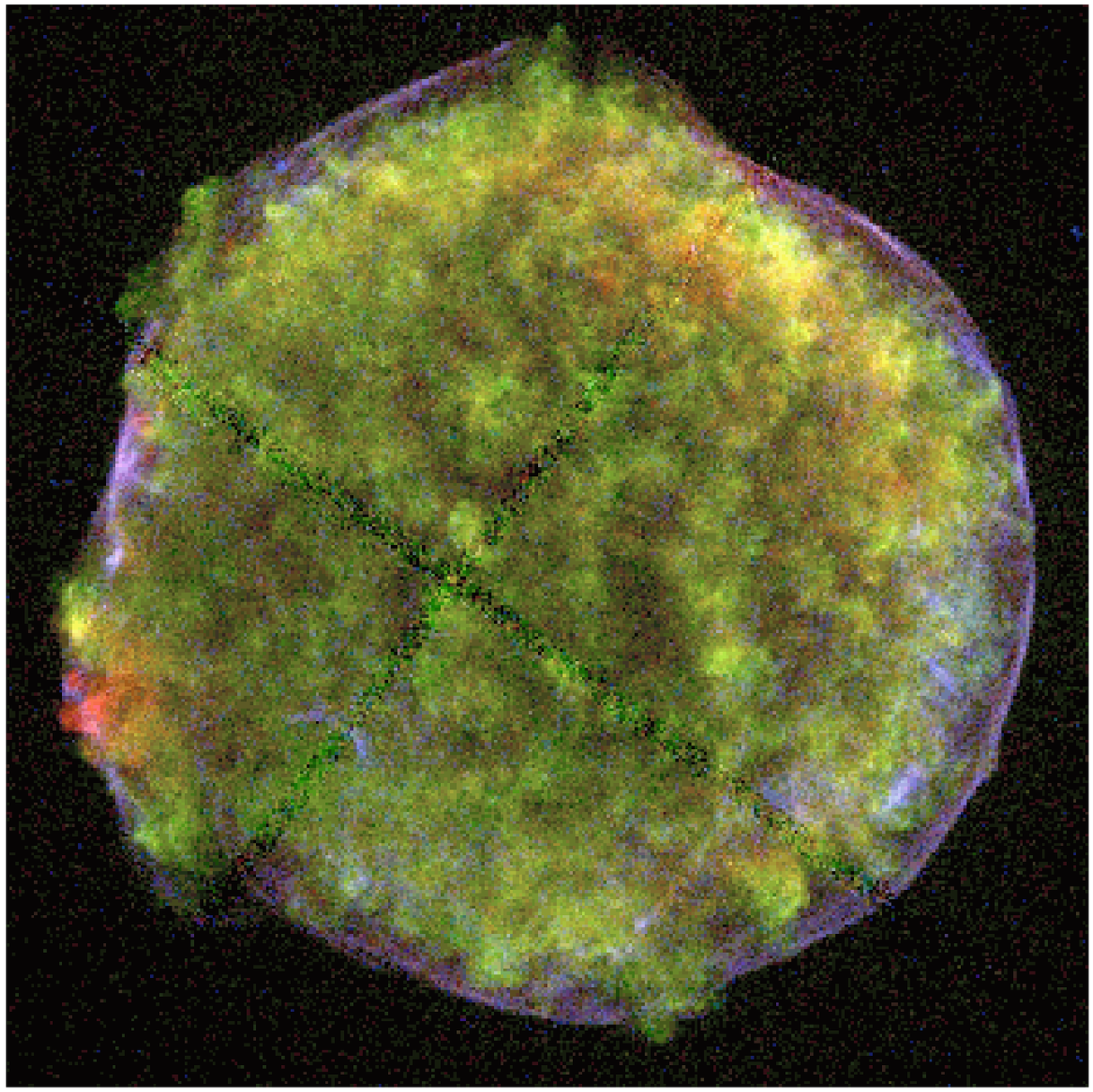

Tycho's SNR viewed in X-rays. The blastwave is marked by the bluish rim (Warren et al. 2005).

EVIDENCE FOR EFFICIENT DSA IN SNRS

- Thin synchrotron rims:

  The radial profile of the X-ray bright synchrotron rims in Tycho can be explained by models for amplified magnetic fields at the shock front and acceleration of electrons to TeV energies.

  Additionally, the synchrotron dominated rims can be used to constrain the ambient medium density to be < 0.6 cm^{-3}.

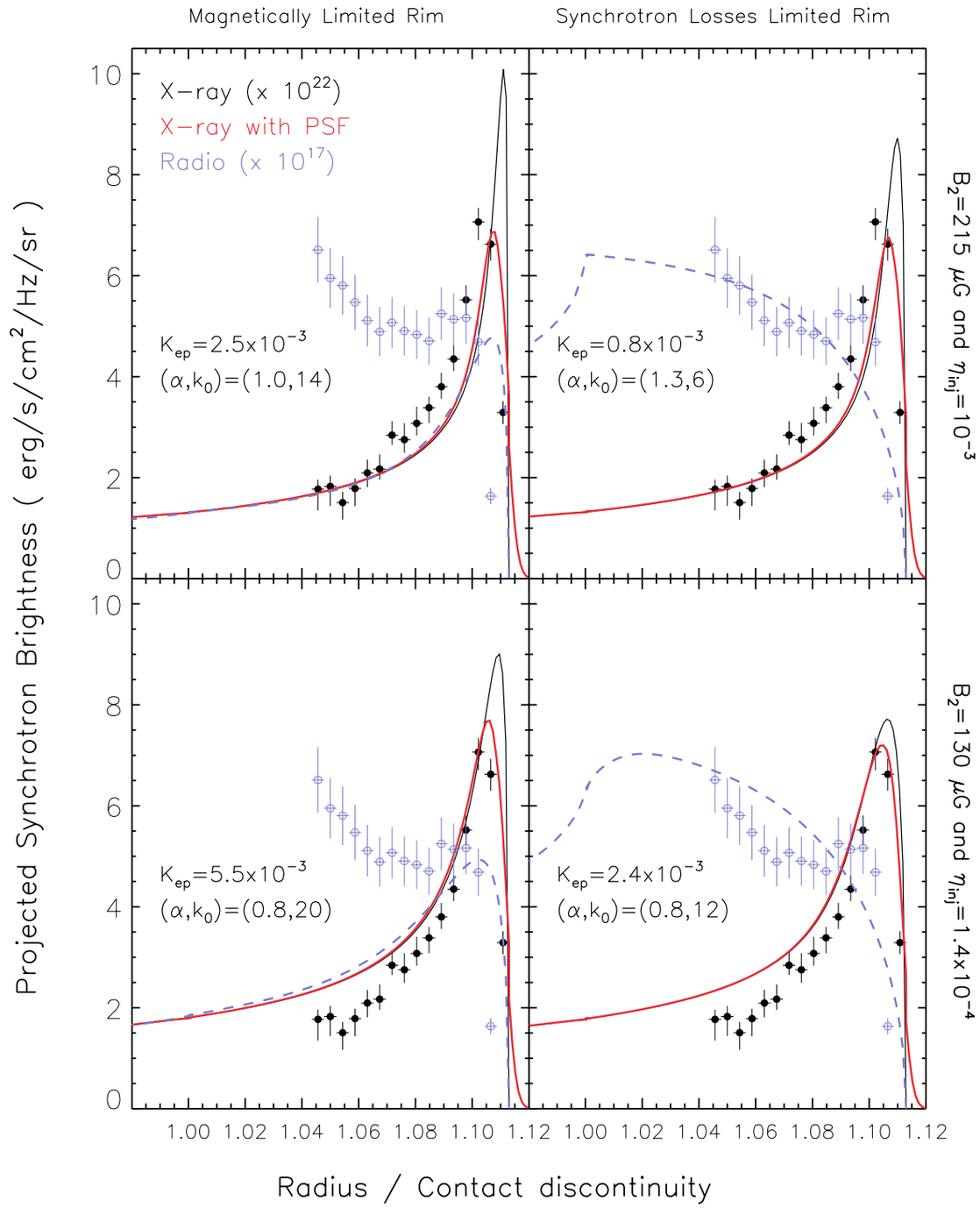

Line of sight projections of radio and X-ray rims with a varying spectral cutoff (α) (Cassam-Chenaï et al. 2007).

EVIDENCE FOR EFFICIENT DSA IN SNRS

- TeV γ -ray emission:

  HESS detections of TeV gamma-rays provides direct evidence for efficient acceleration of particles. However, the origin (leptonic or hadronic) of the TeV gamma rays remains an open question.

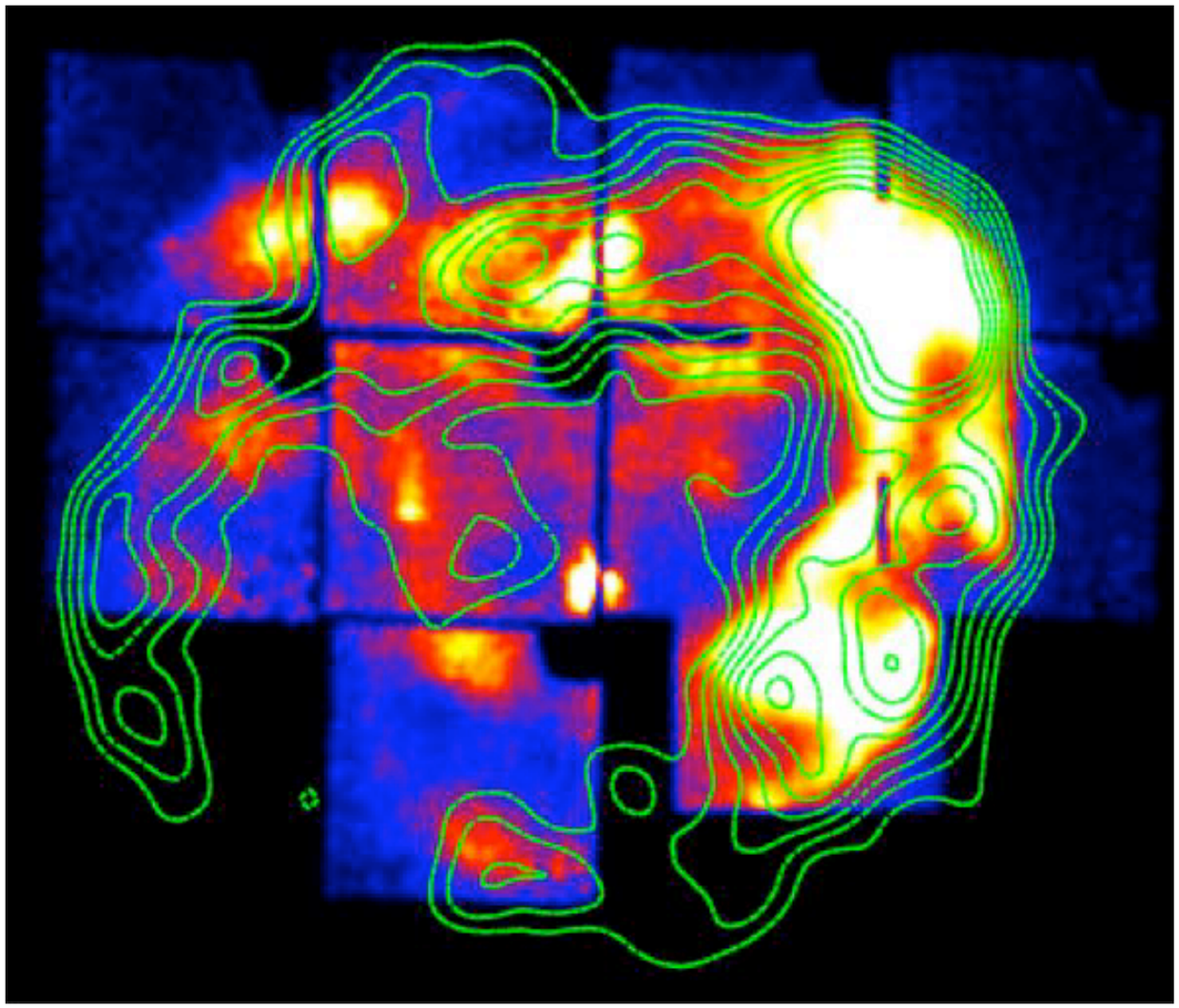

Suzaku XIS image and H.E.S.S. gamma-ray image (contours) of RX J1713-3946. (Left): Broadband SED assuming a hadronic or leptonic origin to the TeV emission (Tanaka et al. 2009).

EVIDENCE FOR EFFICIENT DSA IN SNRS

- TeV γ -ray emission:

  HESS detections of TeV gamma-rays provides direct evidence for efficient acceleration of particles. However, the origin (leptonic or hadronic) of the TeV gamma rays remains an open question.

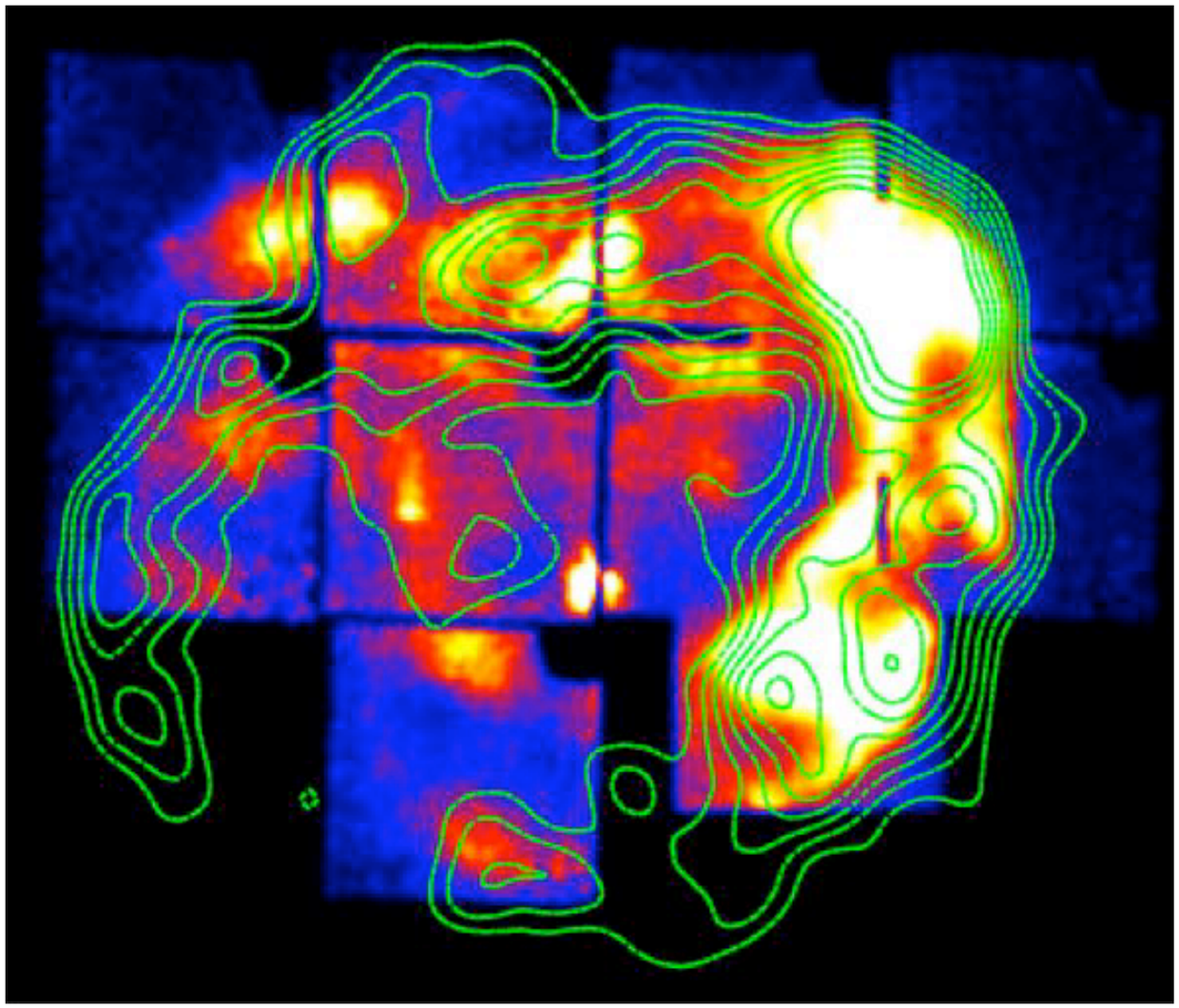

Suzaku XIS image and H.E.S.S. gamma-ray image (contours) of RX J1713-3946. (Left): Broadband SED assuming a hadronic or leptonic origin to the TeV emission (Tanaka et al. 2009).

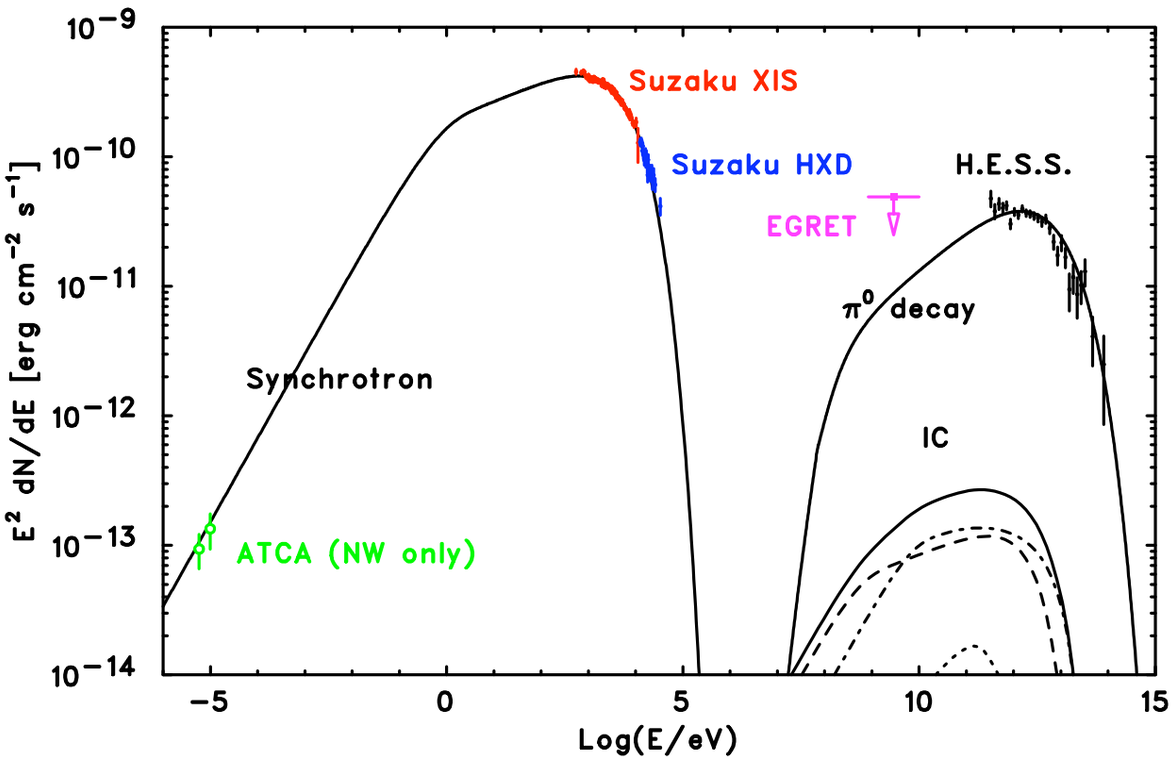

EVIDENCE FOR EFFICIENT DSA IN SNRS

- TeV γ -ray emission:

  HESS detections of TeV gamma-rays provides direct evidence for efficient acceleration of particles. However, the origin (leptonic or hadronic) of the TeV gamma rays remains an open question.

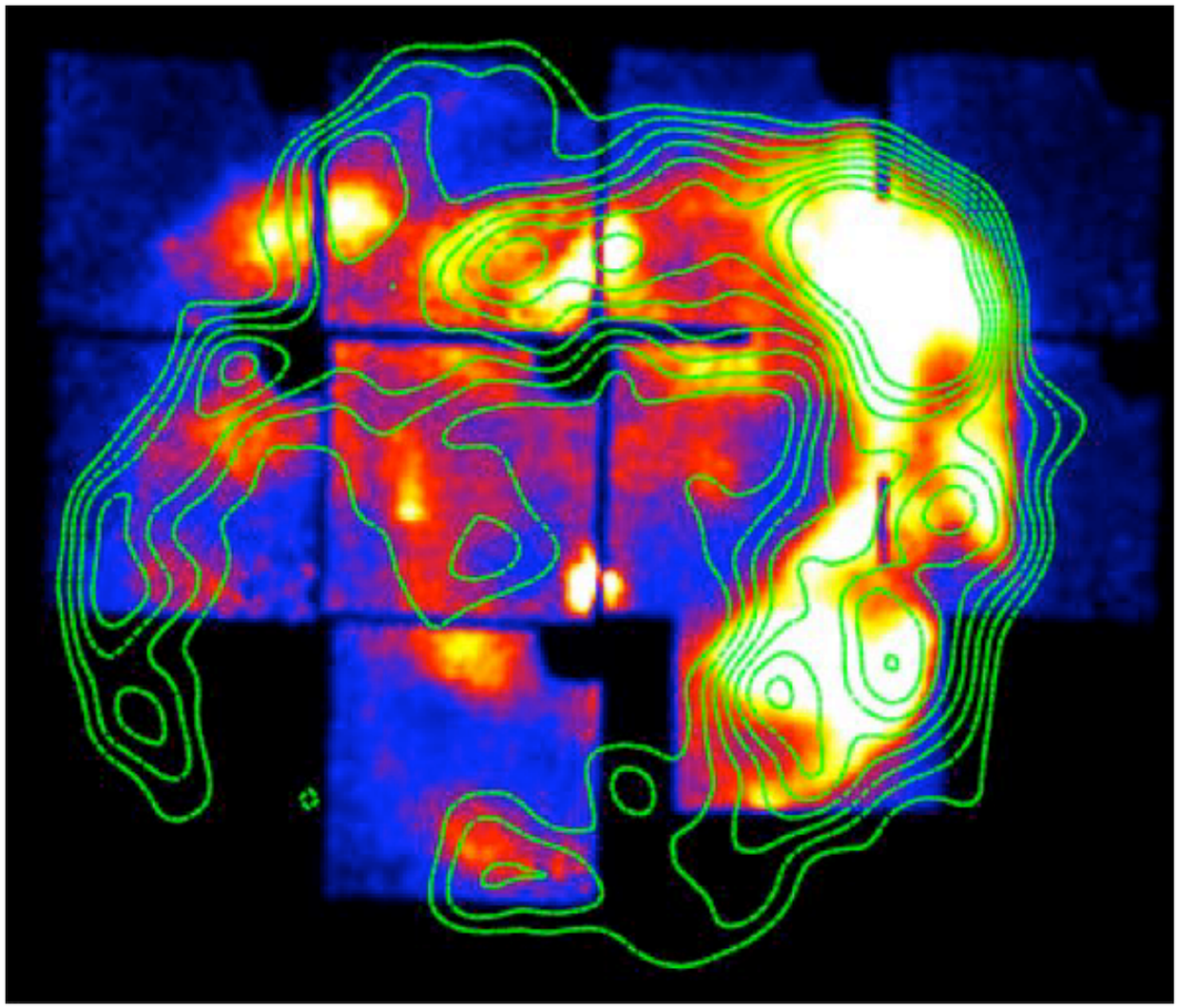

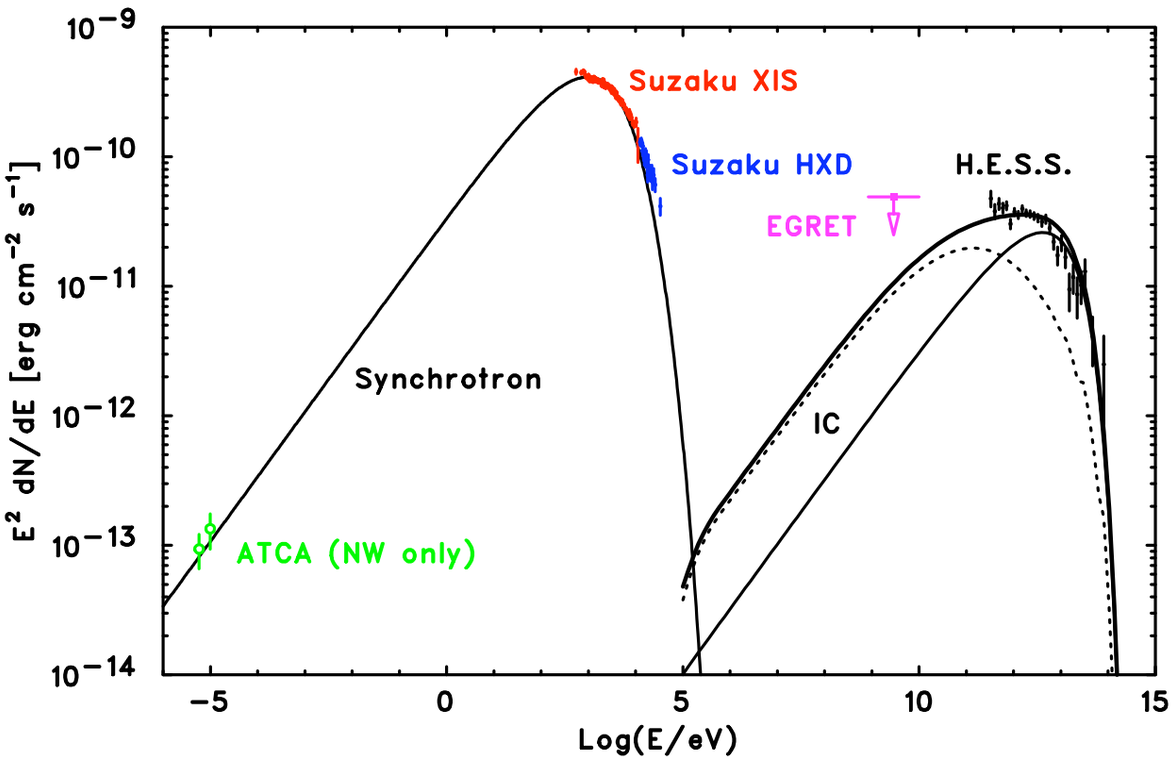

Suzaku XIS image and H.E.S.S. gamma-ray image (contours) of RX J1713-3946. (Left): Broadband SED assuming a hadronic or leptonic origin to the TeV emission (Tanaka et al. 2009).

…AND OTHER EXCITING OBJECTS

…AND OTHER EXCITING OBJECTS

- Supernovae

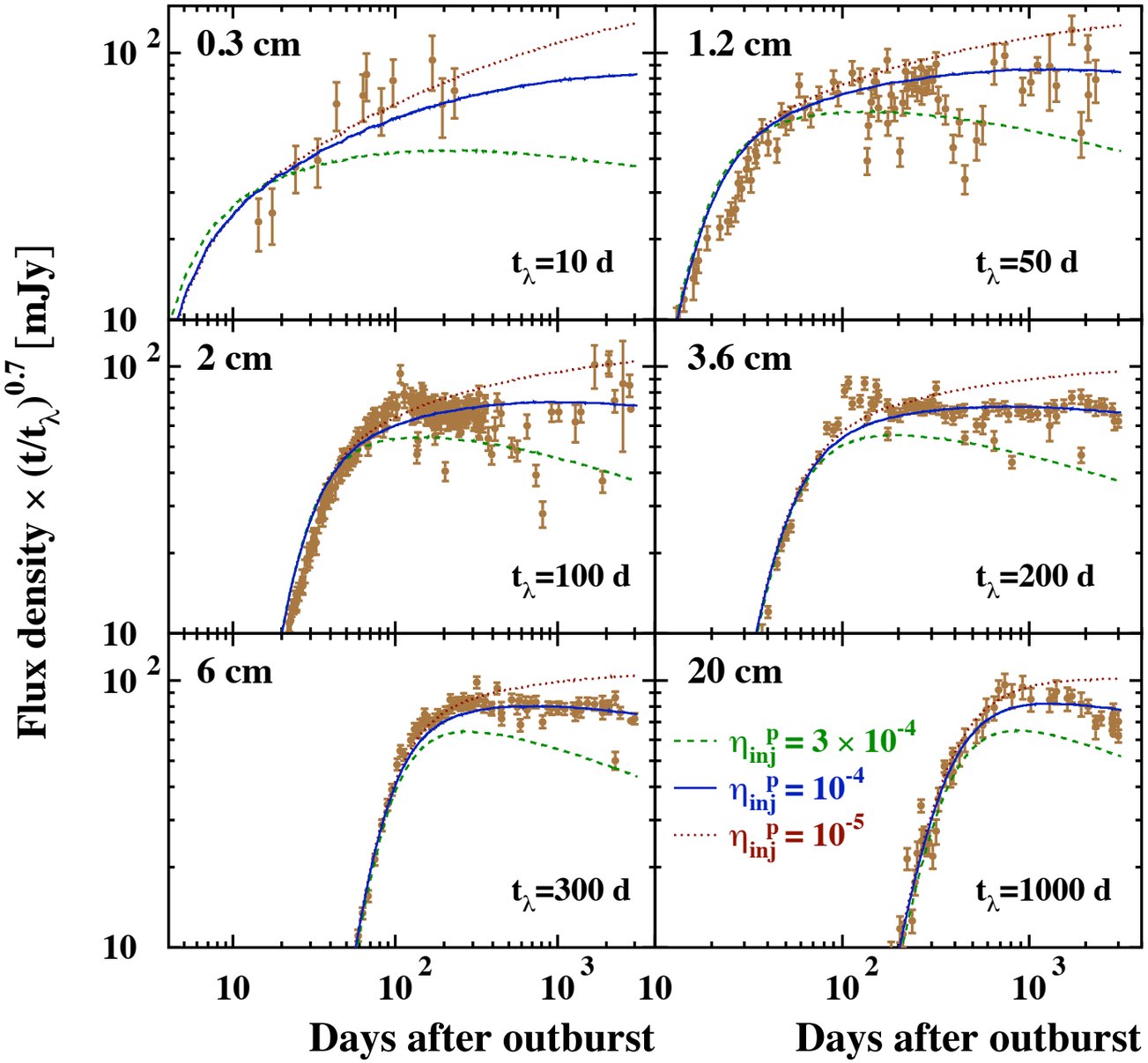

Both the light curve and radio morphology (from VLBI imaging) of SN 1993J suggest that the magnetic field was strongly amplified shortly after explosion. The evolution of the SN indicates that ~ 19% of the total energy in the blastwave was converted to cosmic-ray energy (Tatischeff 2009).

…AND OTHER EXCITING OBJECTS

- Supernovae
- Classical Novae

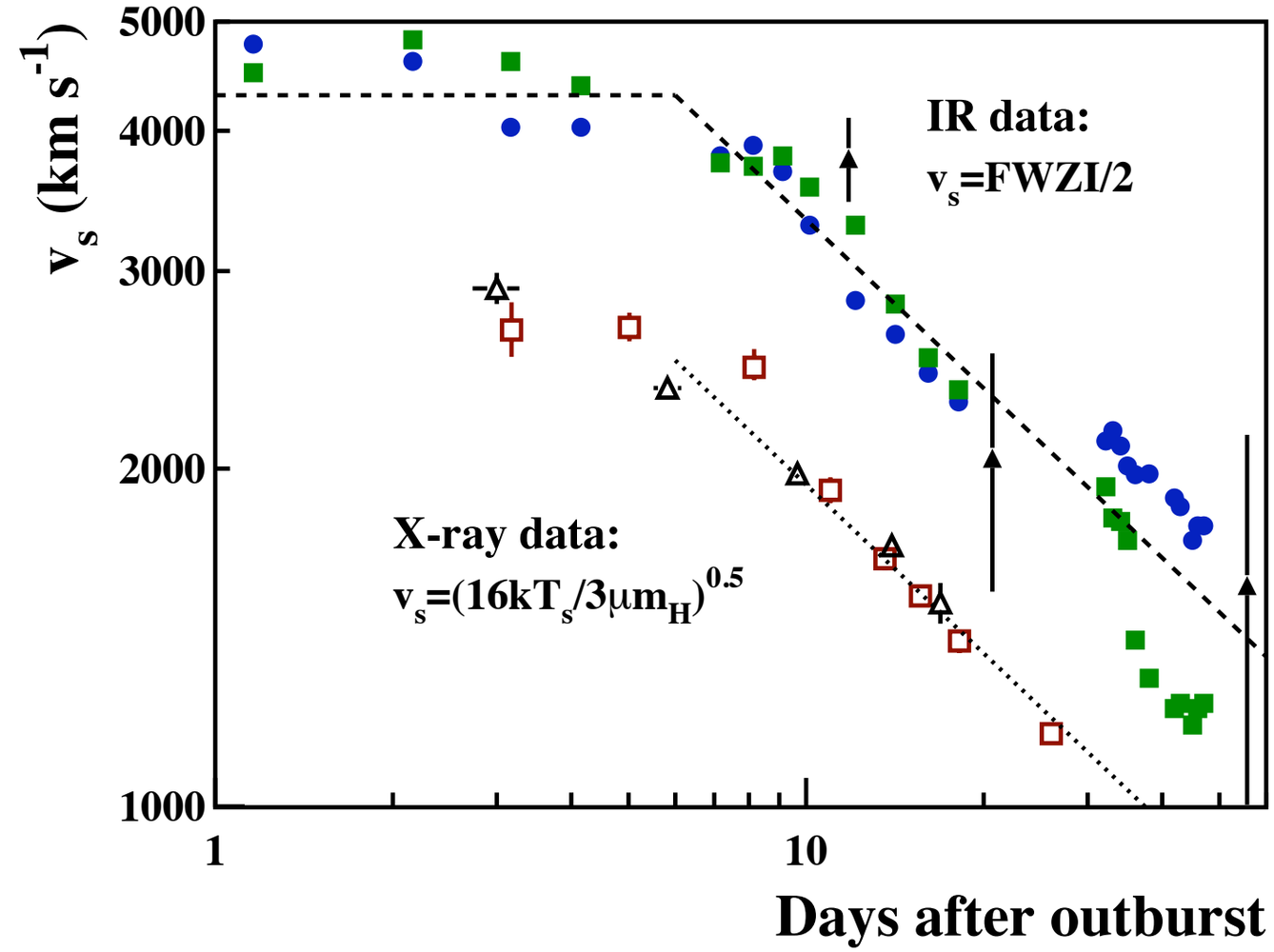

Observations of the 2006 outburst of RS Oph show that the blastwave has decelerated at a rate faster than that predicted from test-particle results. The higher deceleration has been interpreted in the context of efficient acceleration (though there are arguments that a nonspherical outburst would give the same deceleration)

...AND OTHER EXCITING OBJECTS

- Supernovae
- Classical Novae
- AGN

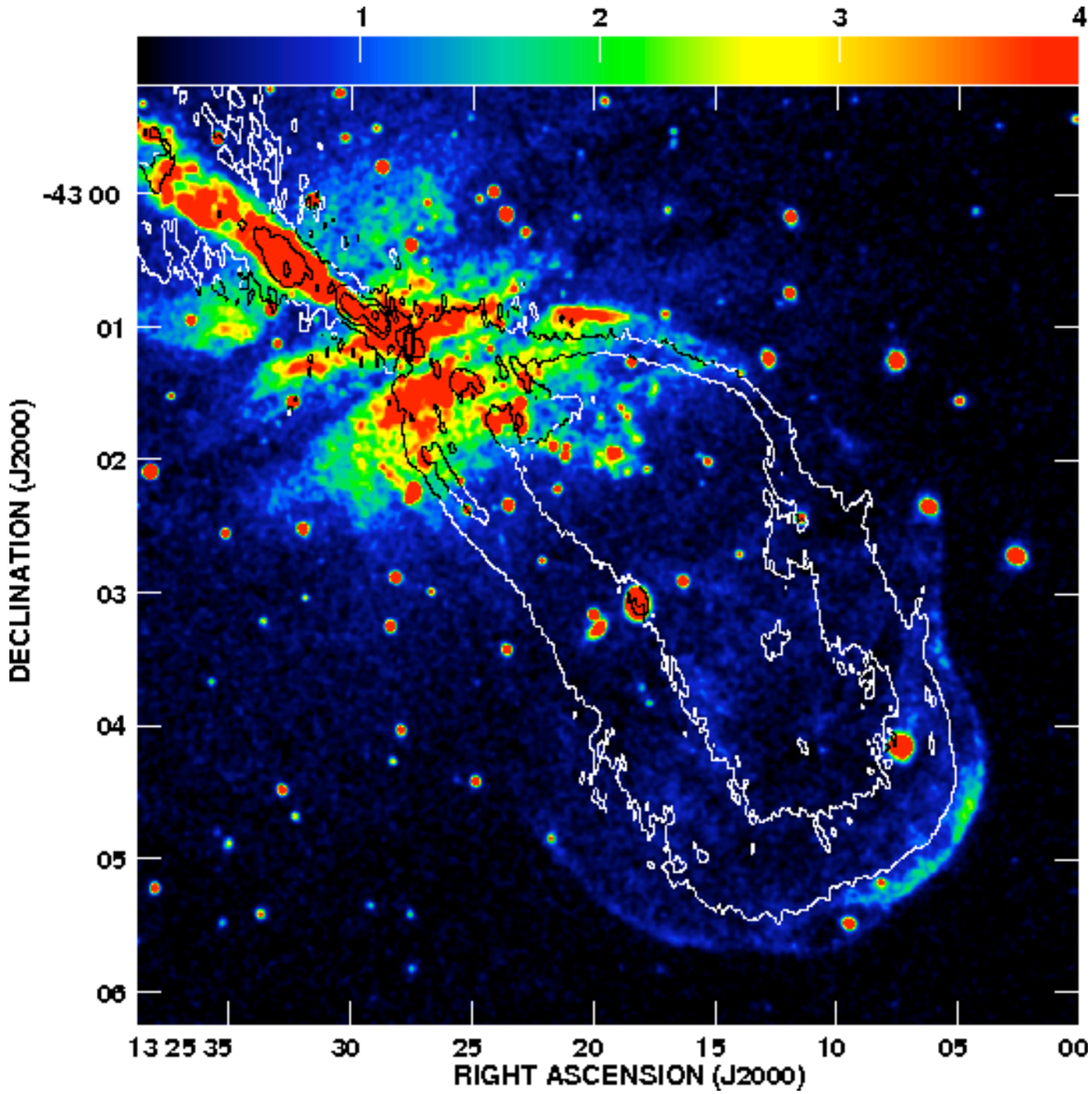

X-ray emission surrounding the SW lobe of Cen A. 1.4 GHz radio contours are shown (Croston et al. 2009).

…AND OTHER EXCITING OBJECTS

- Supernovae
- Classical Novae
- AGN
- Clusters

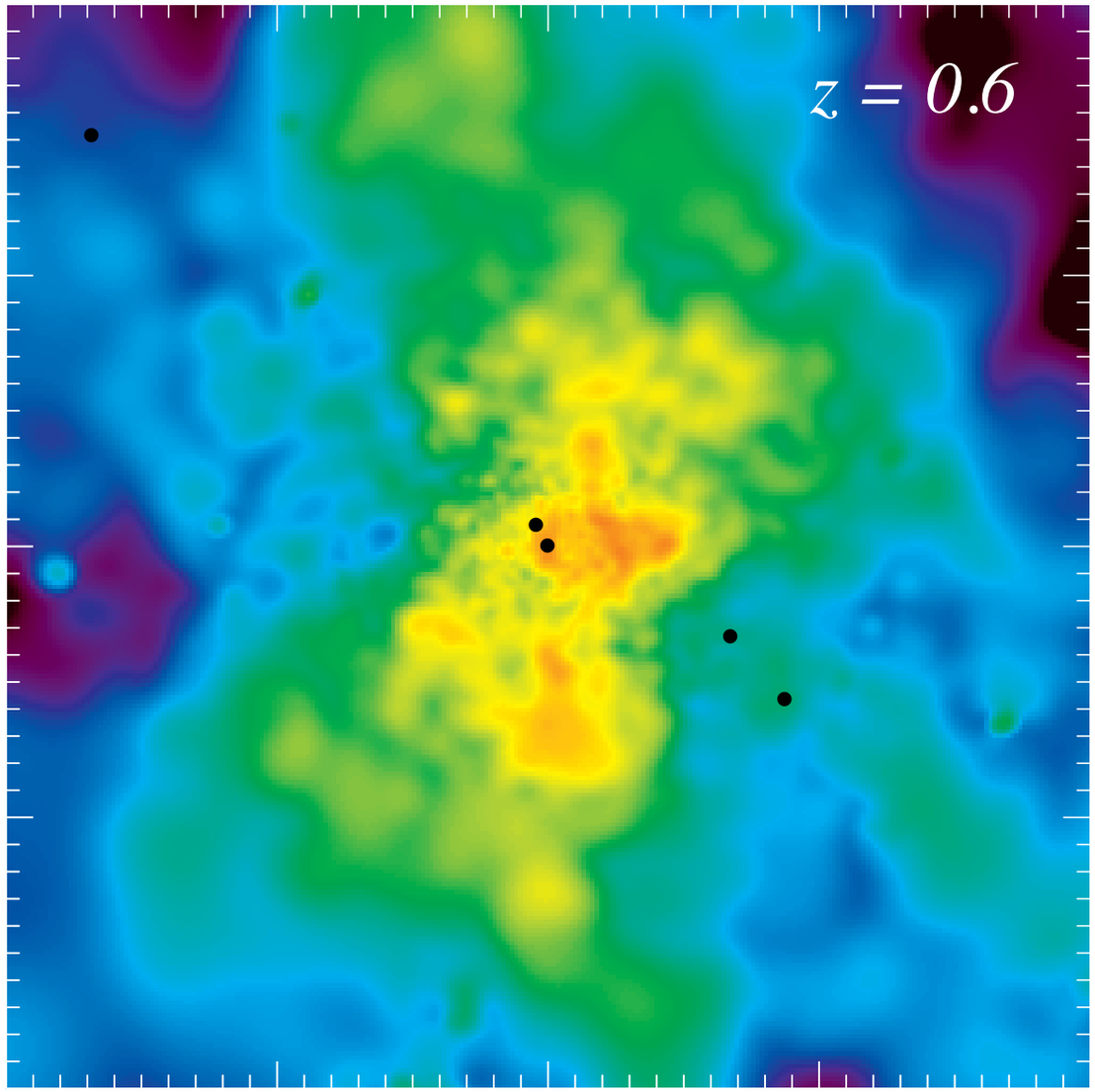

Mass-weighted cosmic ray energy per unit mass at $z = 0.6$ (Sijacki et al. 2008). The box is 4000 h^{-1} kpc on a side.

...AND OTHER EXCITING OBJECTS

- Supernovae
- Classical Novae
- AGN
- Clusters
- ...

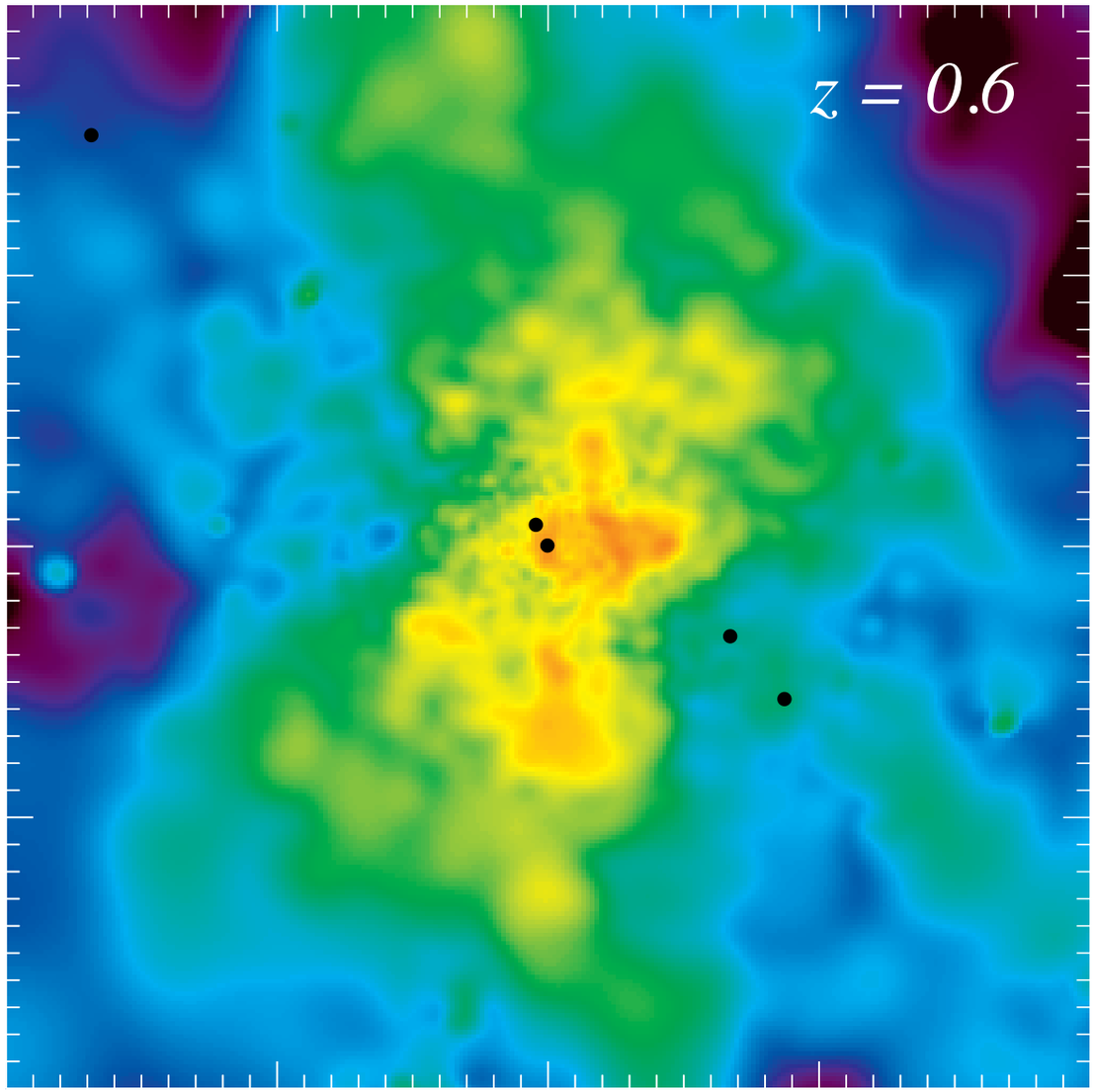

Mass-weighted cosmic ray energy per unit mass at $z = 0.6$ (Sijacki et al. 2008). The box is 4000 h^{-1} kpc on a side.

Existing evidence suggests that in order to understand the morphology of supernova remnants and other exotic astrophysical objects, we need models that self-consistently calculate the hydrodynamics, diffusive shock acceleration, and nonequilibrium ionization in shocks

OUR NEW MODEL: CR+HYDRO+NEI

- Uses semi-analytic model for DSA of Amato & Blasi (2005) and Blasi (2005) coupled to a 1D hydrodynamics code (VH-1)

- The ionization of the shock heated gas at a distance behind the shock is determined by n_e and T_e

- Ionization structure is determined by solving the collisional ionization equations in a Lagrangian gas element

- T_e is calculated by assuming heating via Coulomb collisions, but more efficient heating is considered

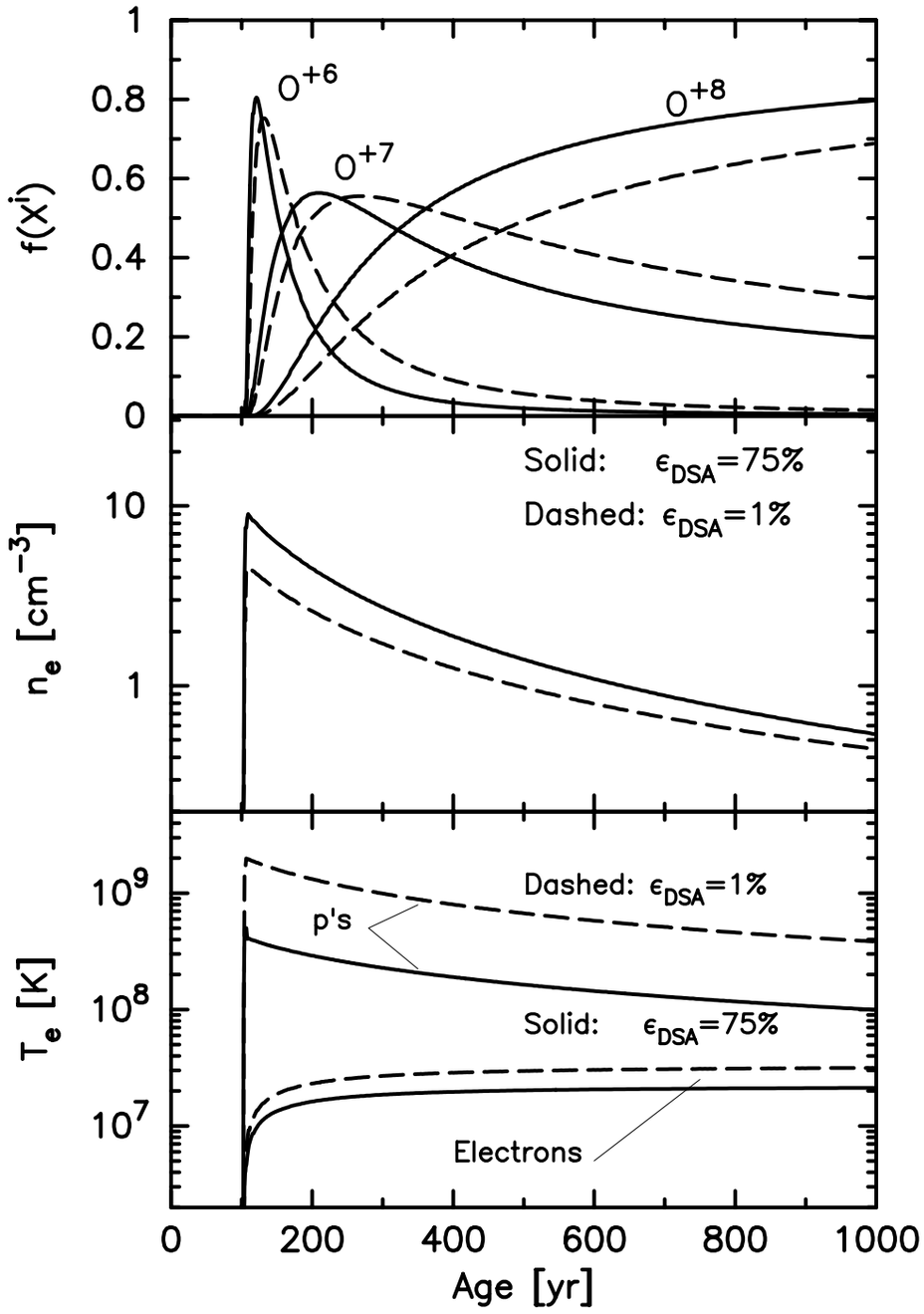

Time evolution of a spherically symmetric Lagrangian mass shell which is crossed by the forward shock at 100 yr. The CSM proton number density for this example is $n_{p,0}$ = 1 cm^{-3}. Here, and in all other examples, the unshocked CSM temperature is T_0 = 10^4 K, and the unshocked magnetic field is B = 15μG.

- Efficient shock acceleration produces a significant nonthermal particle population
- Our model only treats ionizations from the thermal population
- Using a Hybrid model (thermal + power law tail) for the electron distribution, Porquet et al. (2001) showed that nonthermal effects can alter the ionization balance
- The effect is much less pronounced in ionizing plasmas

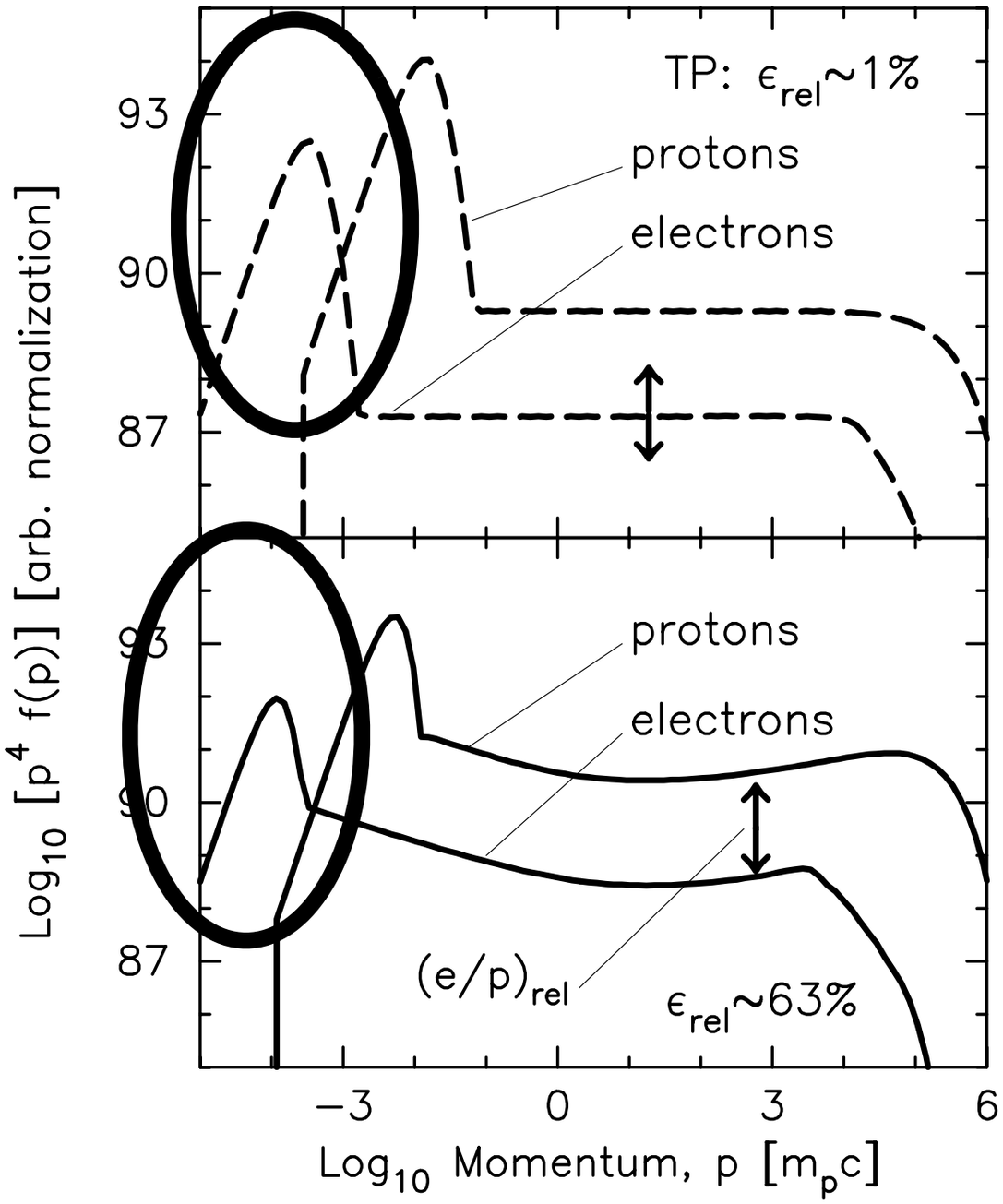

Electron and proton spectra, $p^4 f(p)$, for TP and efficient DSA. The up/down arrow indicates the normalization of the power law component of the distribution. The circled regions indicate the thermal component of the particle distribution functions (Ellison et al. 2007).

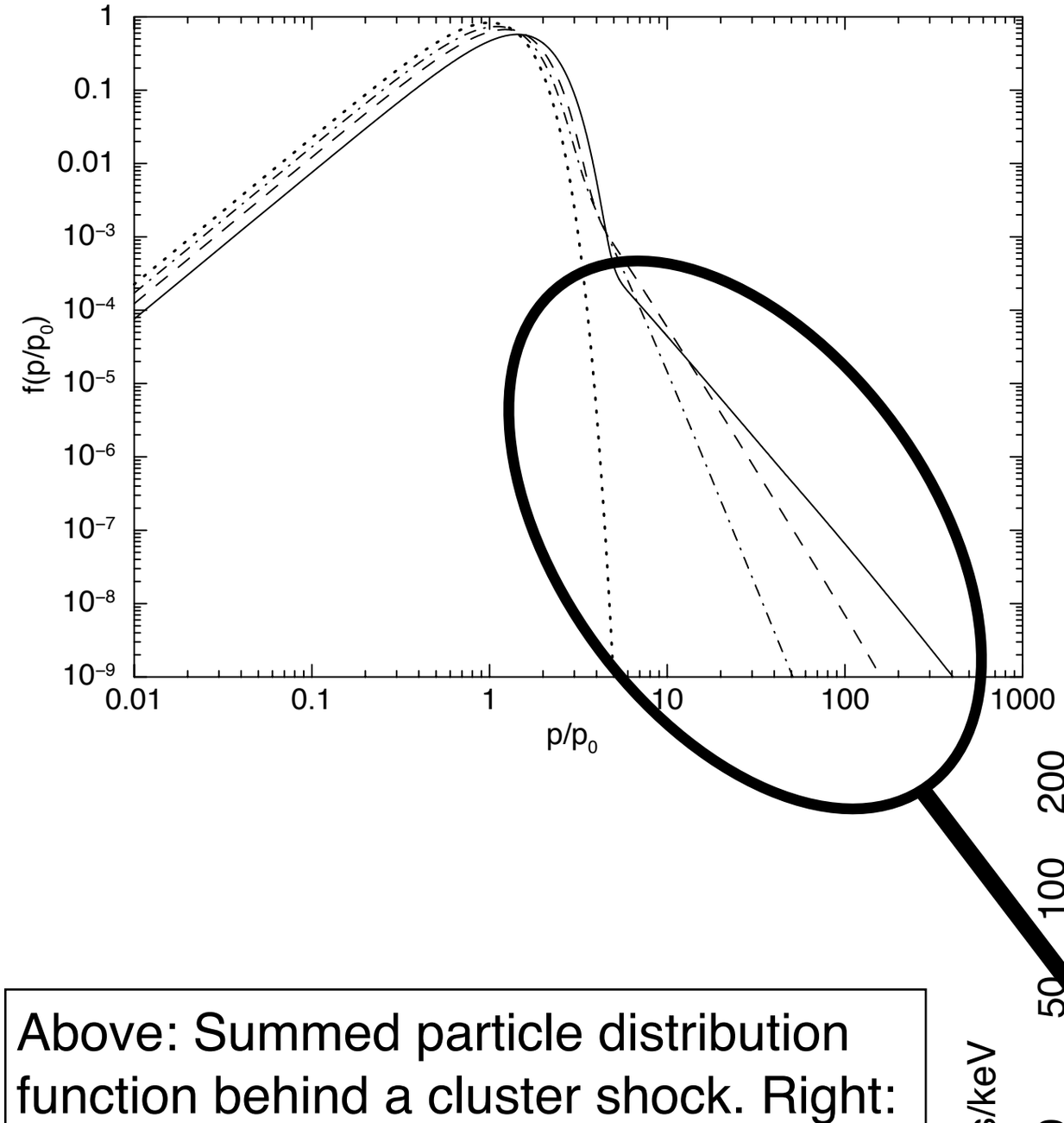

Using a sum of Maxwellians to approximate the particle distribution, Kaastra et al. (2009) showed that the prescence of nonthermal particles alters the relative intensities of satellite lines

Above: Summed particle distribution function behind a cluster shock. Right: Simulated IXO spectrum (crosses) with best fit Maxwellian-plasma model, showing excess at Fe XXV j

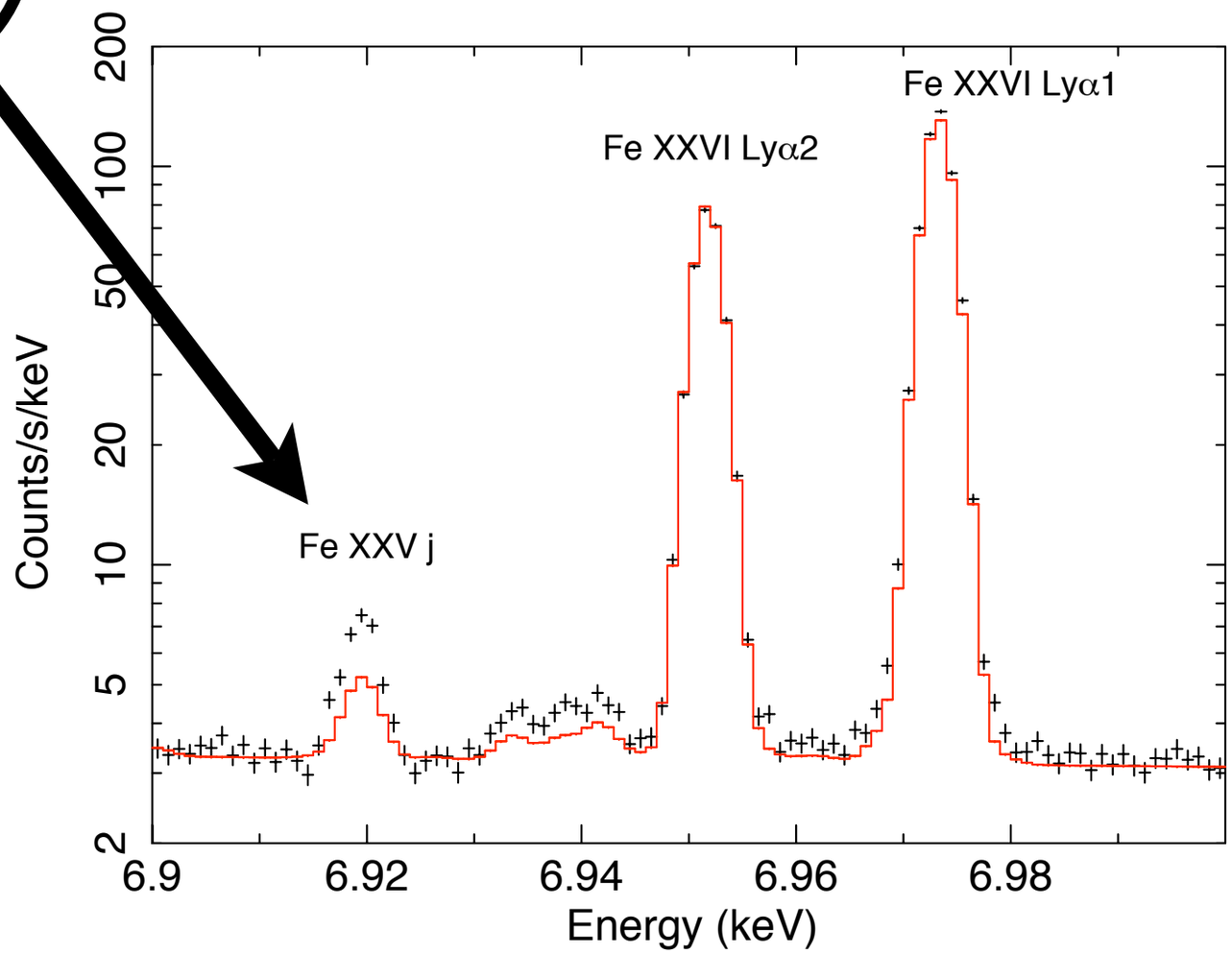

EXAMPLE RESULTS:

- In the efficient models, the charge state for a particular ion peaks closer to the shock front
  - For instance, in the $n_{p,0}$ = 1.0 cm^{-3} models, O^{6+} ~ 2″ behind the FS for efficient models, and ~ 4″ behind for test particle models
- The resolved spatial and spectral structure could provide useful diagnostics for Galactic SNRs undergoing efficient shock acceleration

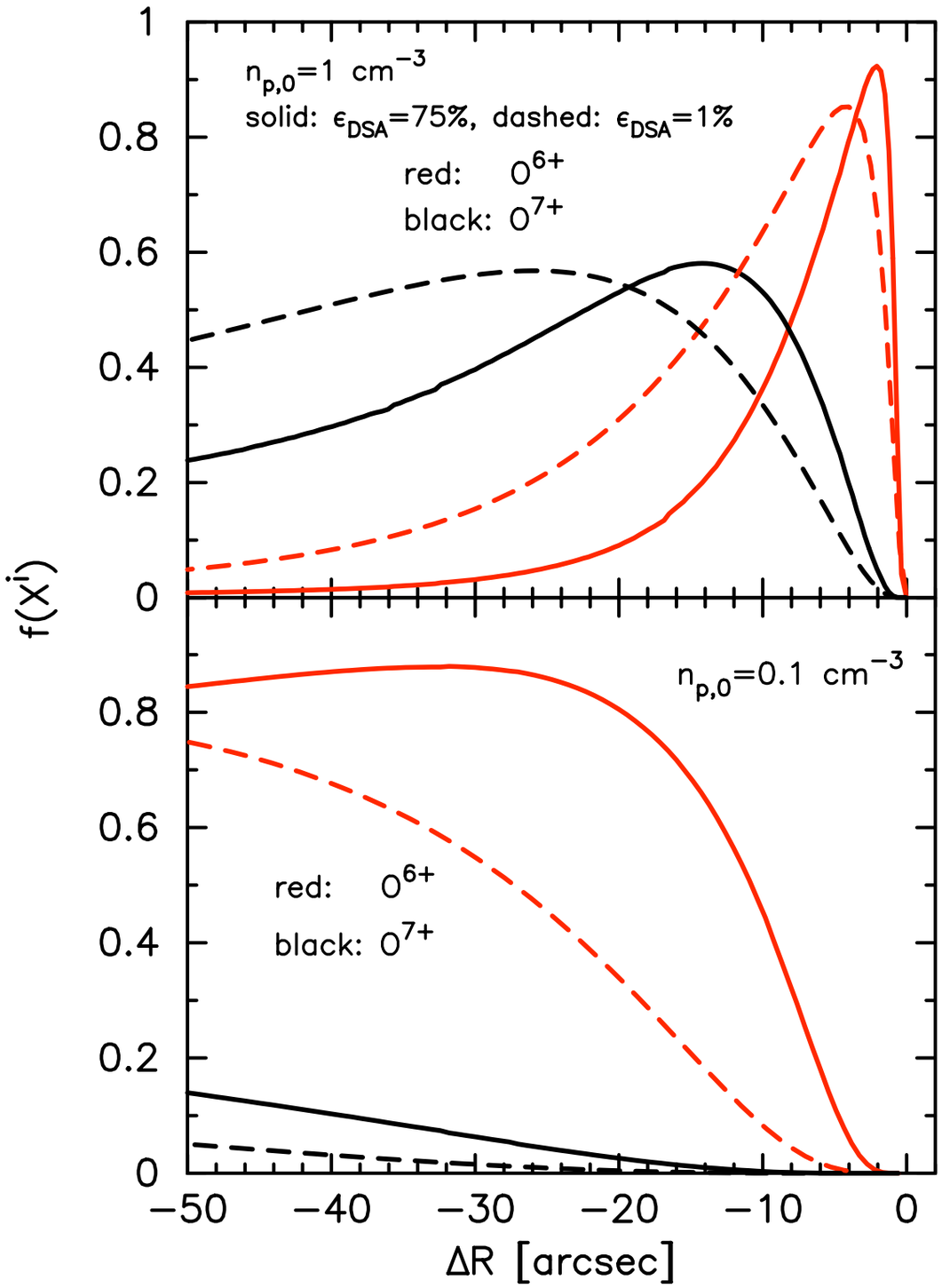

Top: Ionization fraction as a function of distance behind the forward shock for O^{6+} and O^{7+} with $n_{p,0}$ = 1.0 cm^{-3}. Bottom: Ionization fractions of O^{6+} and O^{7+} with $n_{p,0}$ = 0.1 cm^{-3}. In both panels, the solid curves are for ϵ_{DSA} = 75% and the dashed curves are for ϵ_{DSA} = 1%. The angular scale is determined assuming the SNR is at a distance of 1 kpc and the results are calculated at t_{SNR} = 1000 yr.

IONIZATION AGE VS ACCELERATION EFFICIENCY:

- Simulation also tracks ionization age ($n_e t$)
- For increasing acceleration efficiency, SNRs appear to have a higher ionization age
- SNR shocks also have a smaller radius and appear younger in the efficient case
- Additionally, test-particle models with higher E_{sn} can appear spectrally similar to models with lower E_{sn} but differing acceleration efficiencies

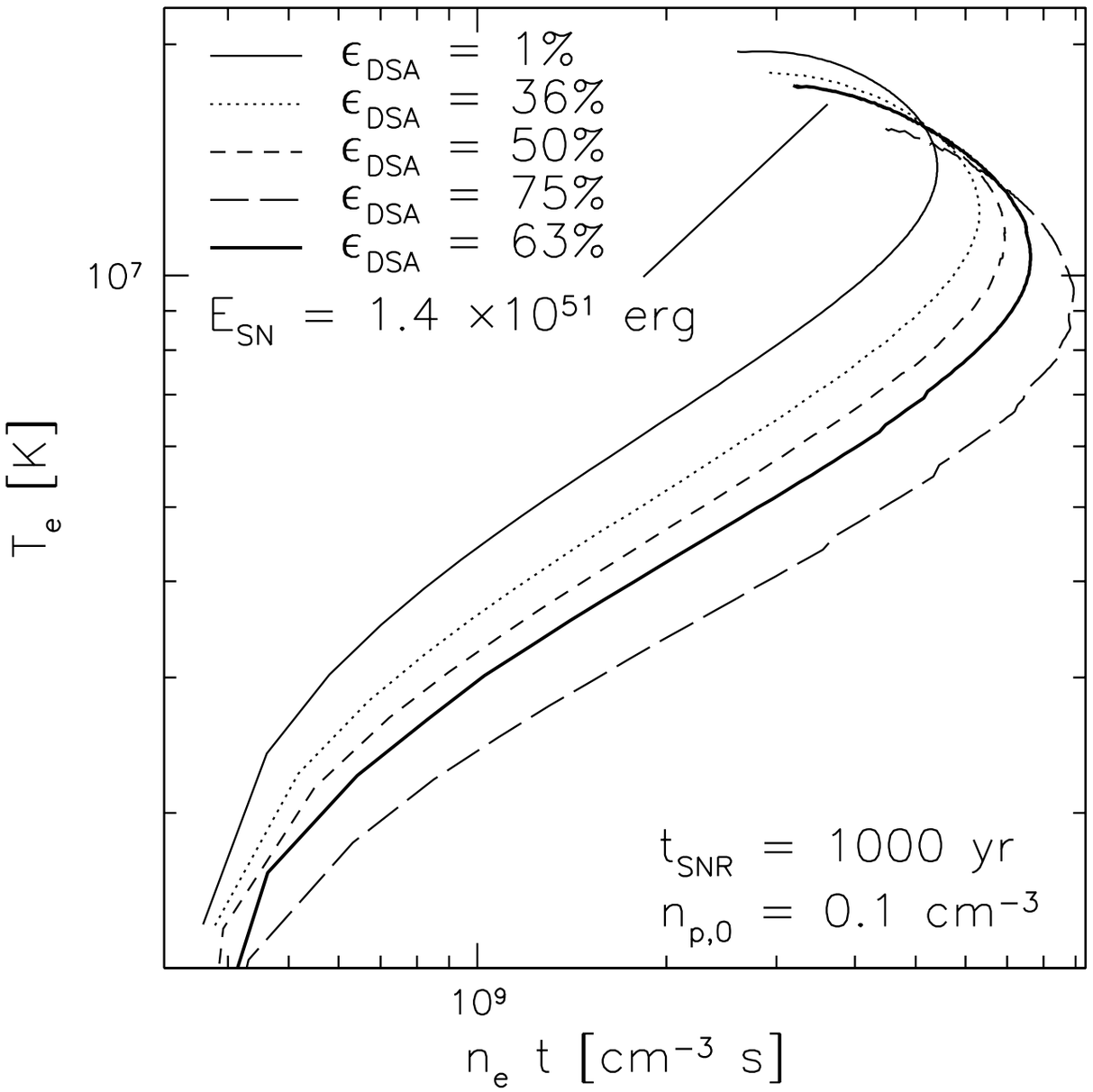

$n_e t$ vs T_e for varying acceleration efficiency. In these curves, the forward shock is in the lower left, and the contact discontinuity is at the upper right.

EXAMPLE RESULTS:

$E_{sn} = 10^{51}$ erg
$M_{ej} = 1.4 M_{sun}$
constant density
ambient medium

EXAMPLE RESULTS:

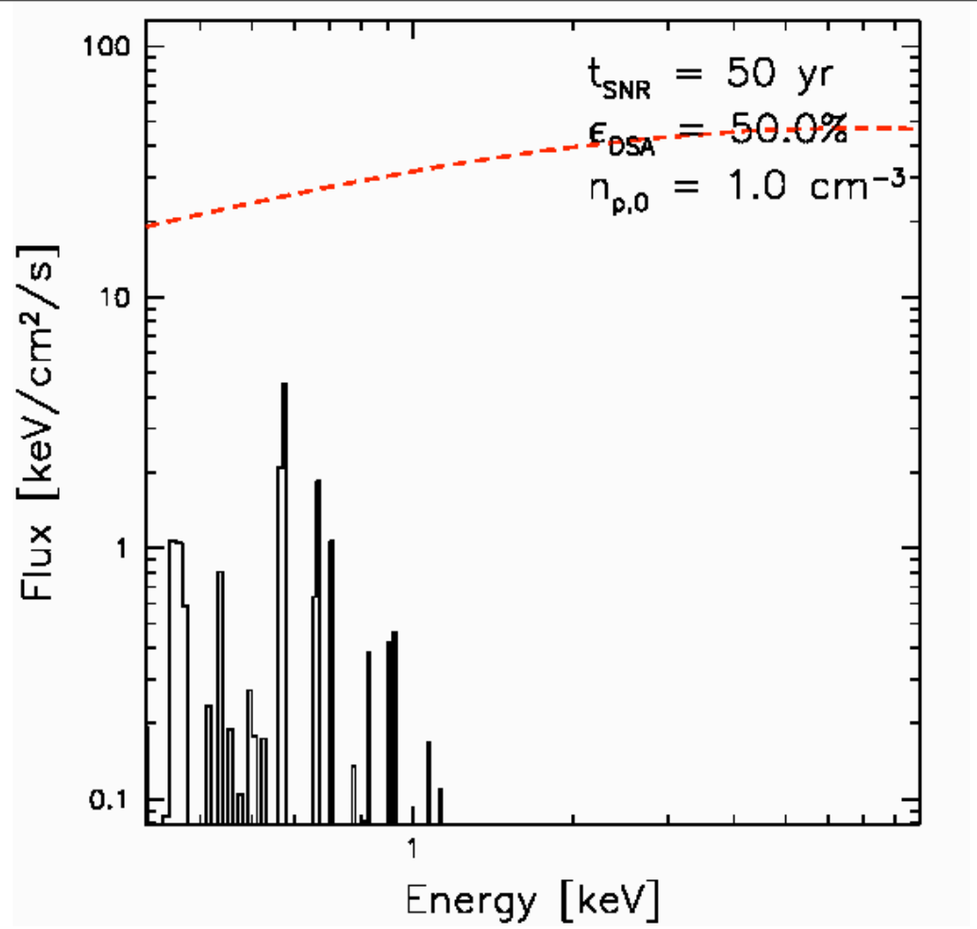

$E_{sn} = 10^{51}$ erg
$M_{ej} = 1.4 M_{sun}$
constant density
ambient medium

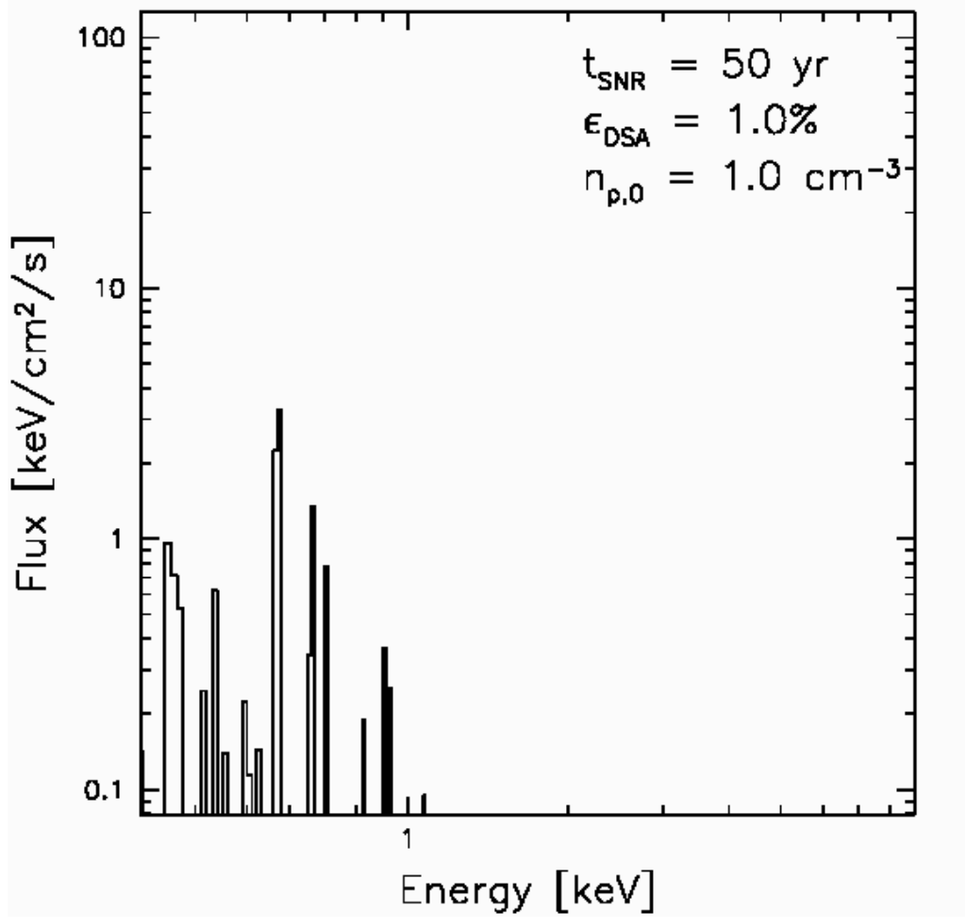

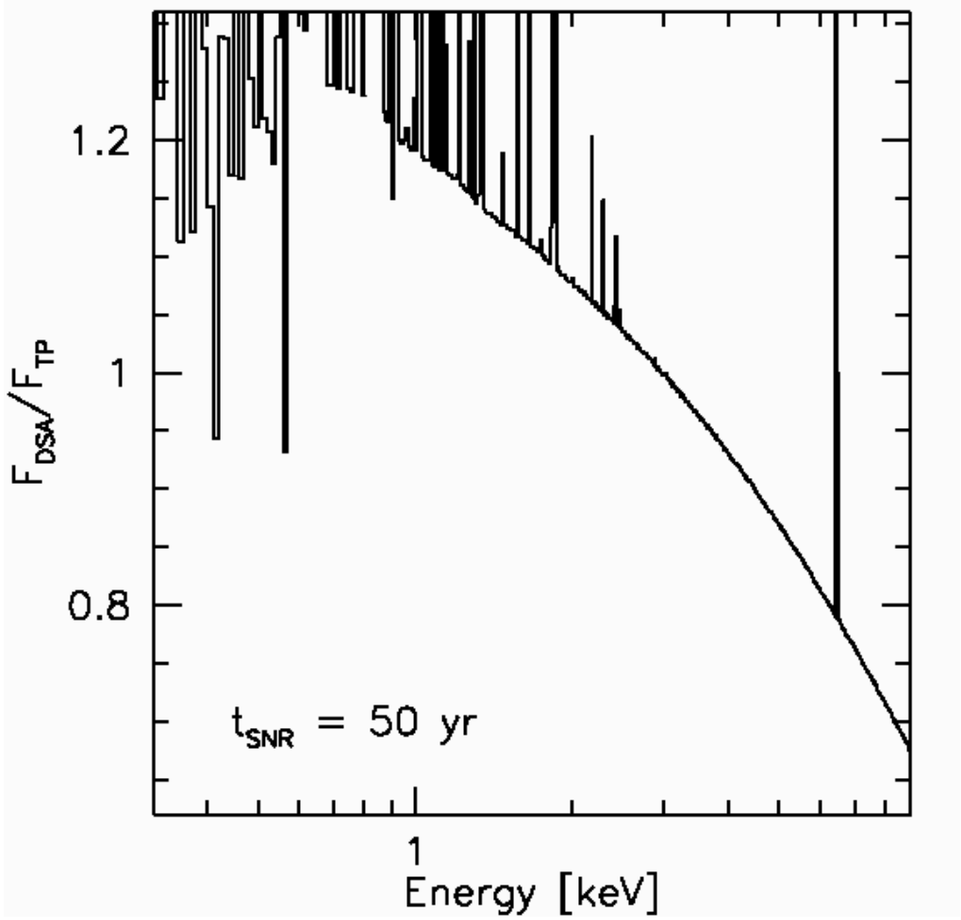

EXAMPLE RESULTS:

$E_{sn} = 2 \times 10^{51}$ erg

$M_{ej} = 2 M_{sun}$

$\dot{M} = 2 \times 10^{-5}\ M_{sun}\ yr^{-1}$

$v_{wind} = 10\ km\ s^{-1}$

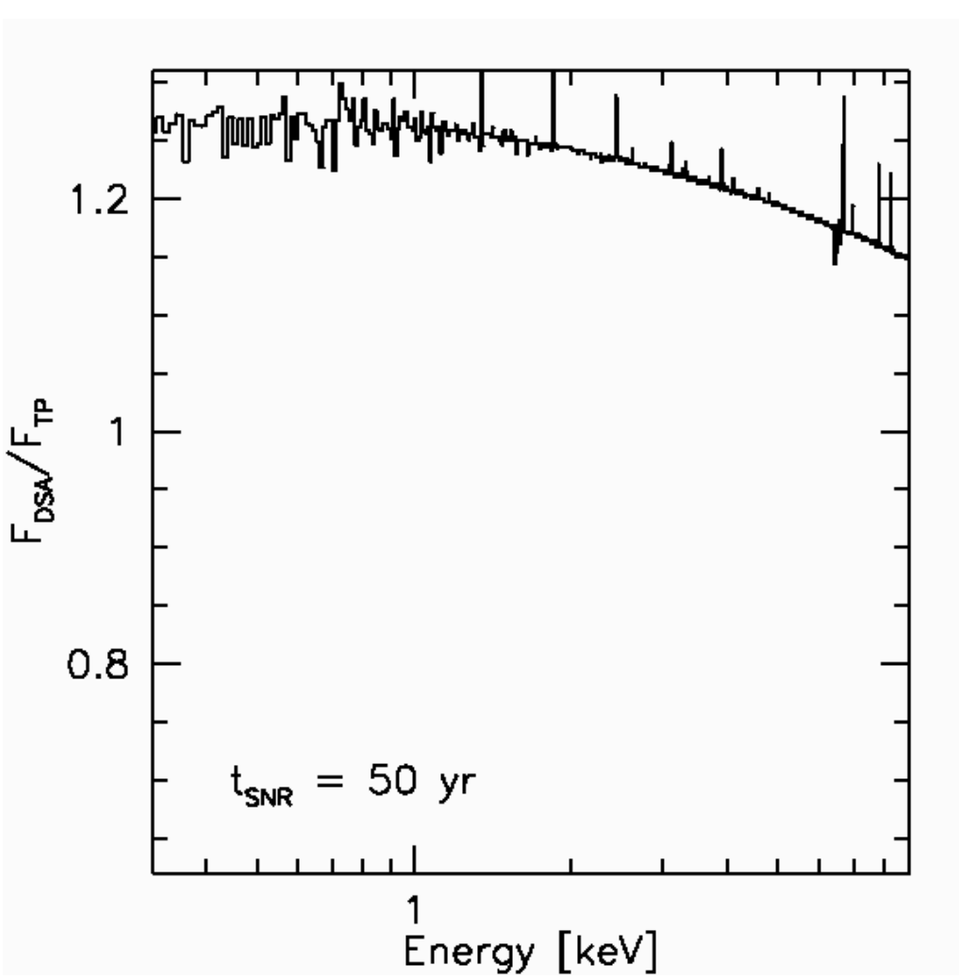

EXAMPLE RESULTS:

$E_{sn} = 2 \times 10^{51}$ erg

$M_{ej} = 2M_{sun}$

$\dot{M} = 2 \times 10^{-5}\ M_{sun}\ yr^{-1}$

$v_{wind} = 10\ km\ s^{-1}$

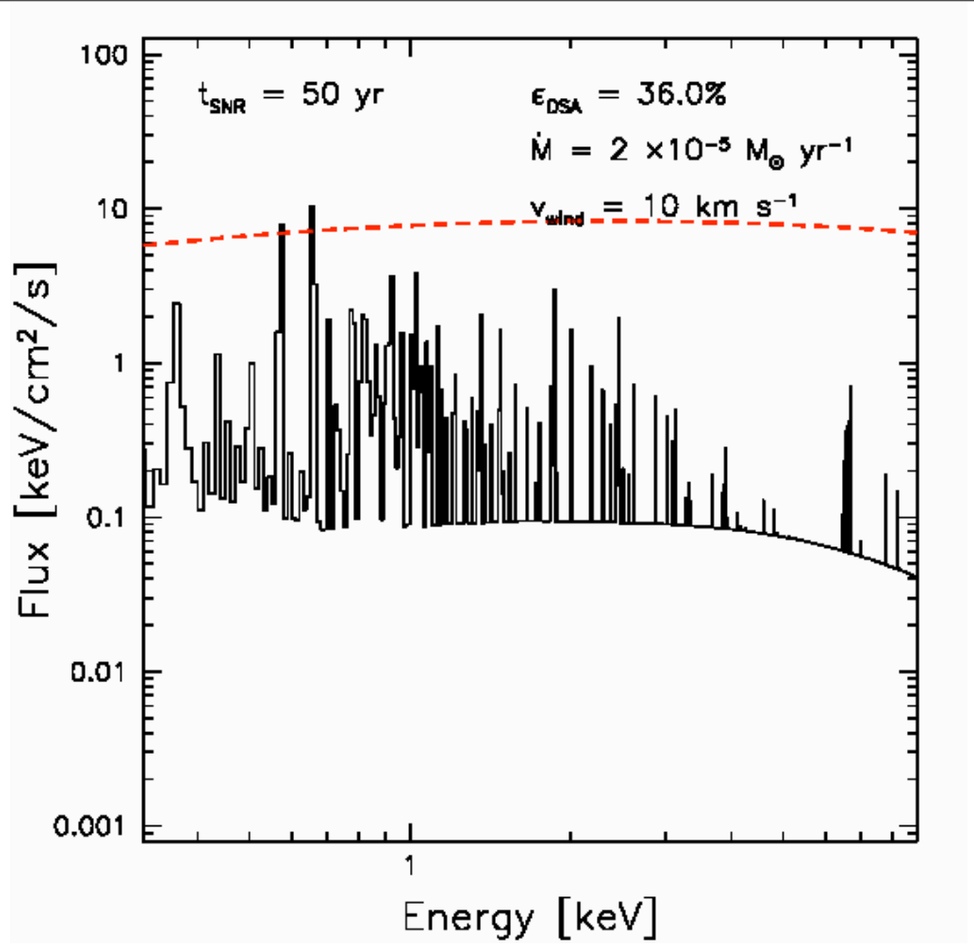

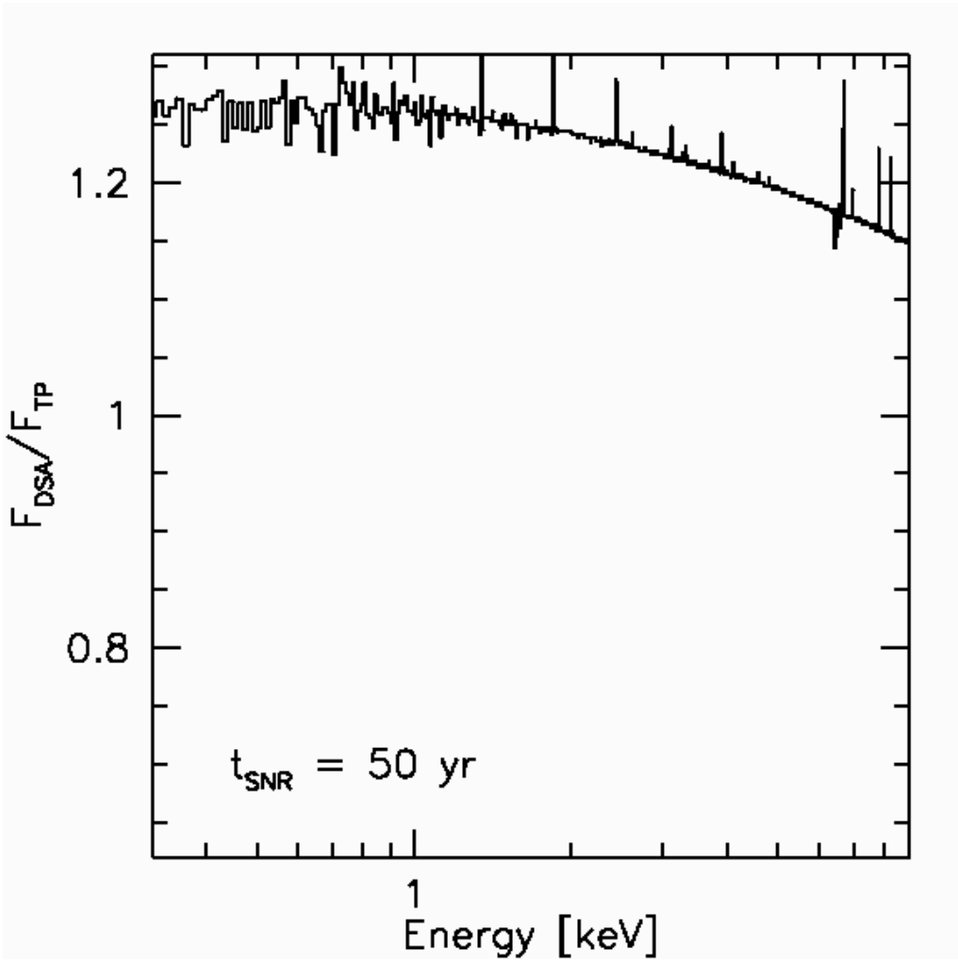

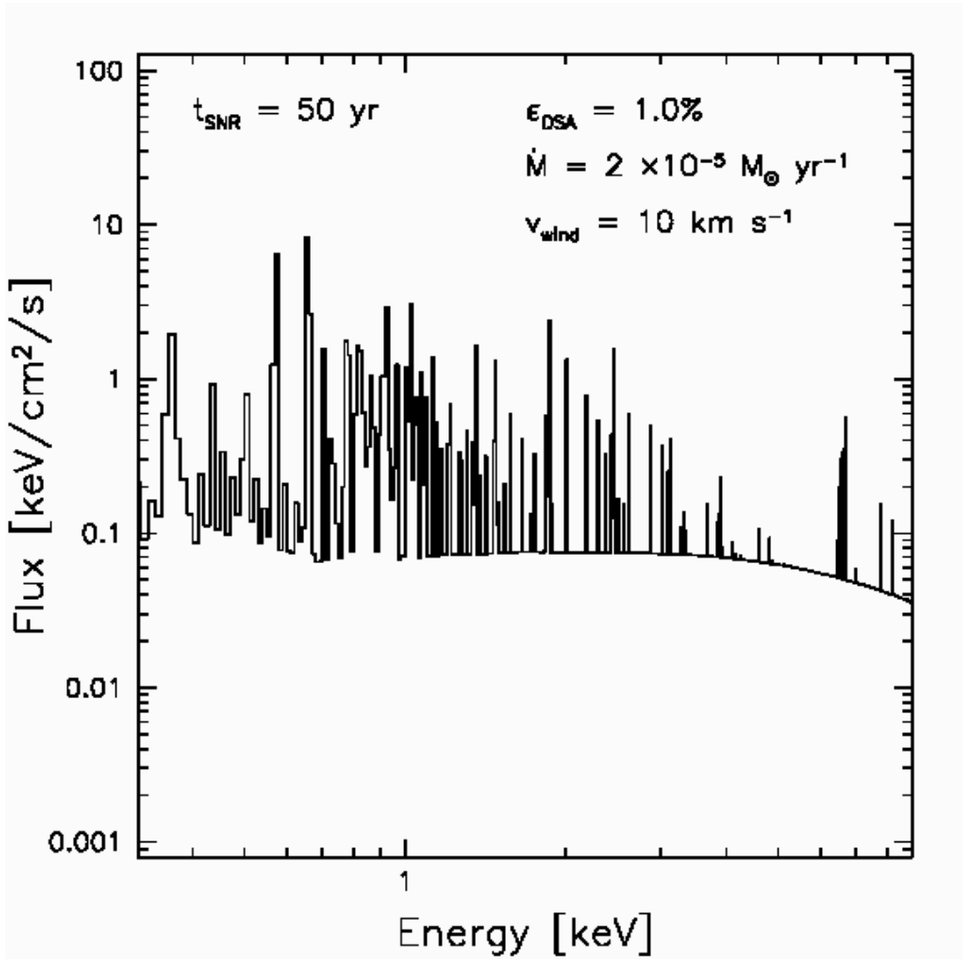

EXAMPLE RESULTS:

$E_{sn} = 2 \times 10^{51}$ erg

$M_{ej} = 2M_{sun}$

$\dot{M} = 2 \times 10^{-5}\ M_{sun}\ yr^{-1}$

$v_{wind} = 10\ km\ s^{-1}$

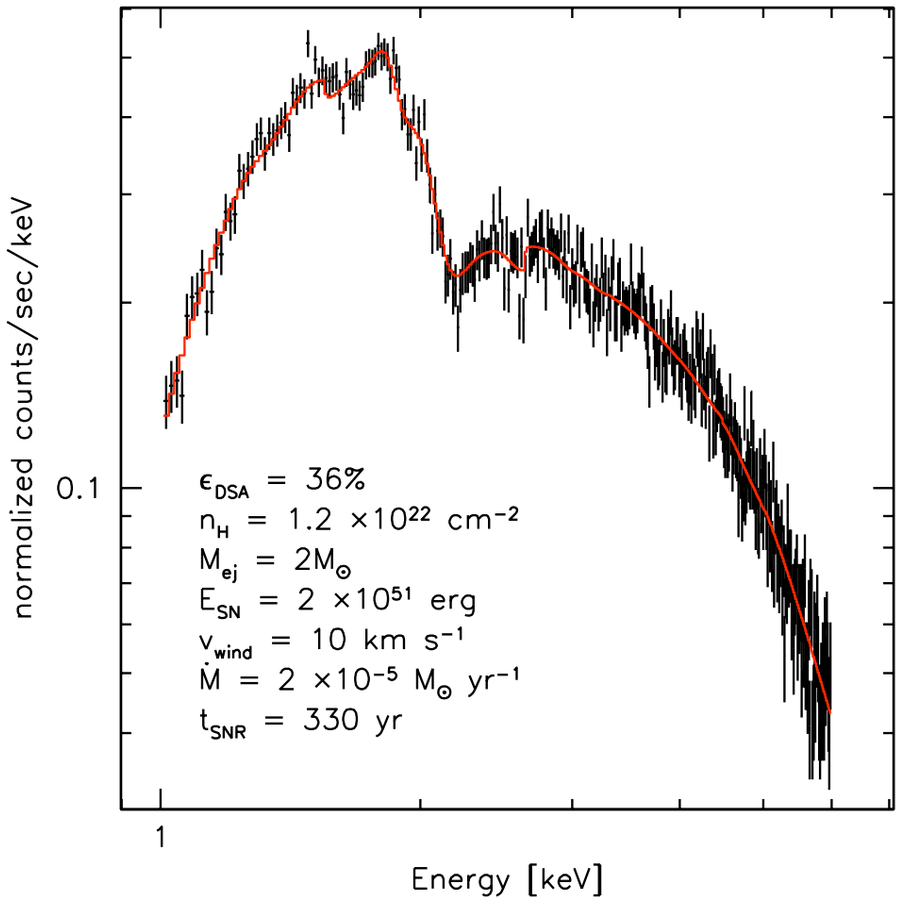

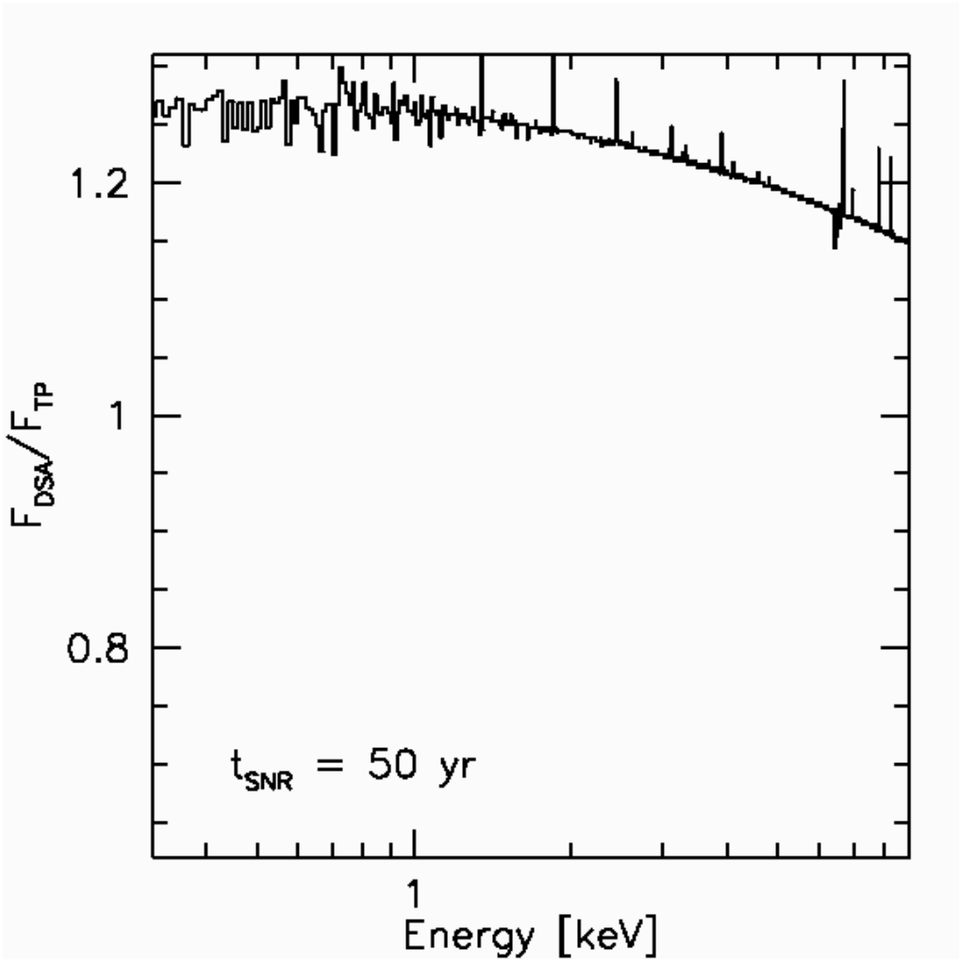

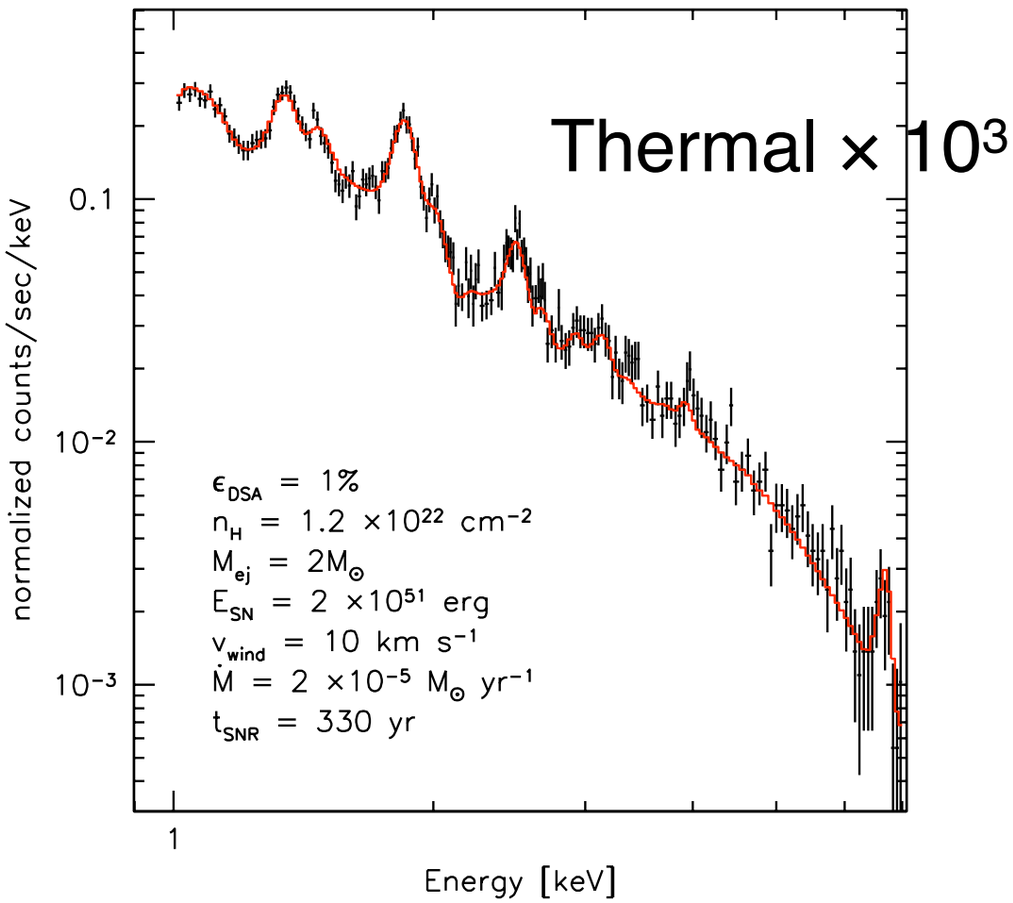

CONCLUSIONS:

- Efficient cosmic-ray production via DSA significantly alters the NEI of material behind the SNR blastwave
- Because of higher postshock densities, higher charge states are reached at lower electron temperatures
- The spatial structure of the ionization varies with acceleration efficiency. This is reflected in the emitted thermal X-ray spectrum
- Future work includes:
  - SN ejecta composition
  - DSA at the SNR reverse shock (Helder & Vink, 2008; Uchiyama et al. 2008)